Pulmonary Hypertension Promotes Neuroinflammation and Neurodegeneration

Priscilla M. De La Cruz[1,2], Angelia Lockett[1], Marta T. Gomes[1], Somanshu Banerjee[3], Asif Razee[3], Amanda Fisher[1], Todd Cook[1], Christopher D. Lloyd[4], Shino Magaki[5], Soban Umar[3], Adrian L. Oblak[4], Roberto F. Machado[1*]

[1] Division of Pulmonary, Critical Care, Sleep and Occupational Medicine, Indiana University, Indianapolis

[2] Division of Pulmonary, Critical Care, and Sleep Medicine, University of New Mexico, Albuquerque

[3] Department of Anesthesiology, University of California Los Angeles Health, Los Angeles

[4] Stark Neuroscience Research Institute, Indianapolis

[5] Department of Pathology and Laboratory Medicine, University of California, Los Angeles

The authors declare no competing interests. Artificial intelligence was used to debug R code (ChatGPT) and proofread paper (Paperpal).

*Correspondence to: Roberto Machado, 980 W Walnut Street, Room C400, Walther Hall, R3, Indianapolis, IN 46202, robmacha@iu.edu, 317-278-0047(Phone), 317-278-7030 (Fax)

Author Contributions:

PD- Designed and performed experiments, data analysis, manuscript preparation, AL-Performed and interpreted cell culture experiments, MG-Performed and interpreted cell culture experiments, SB- Performed antibody validations, immunostaining and microscopy, AR- Performed antibody validations, immunostaining and microscopy, AF- Managed animal colonies, TC- Performed and interpreted right heart catheterization, CL-Assisted with design of immunohistochemistry experiments, SM- Experimental design, technical expertise, SU-

Funding: NIH T32-HL091816(PD), AHA-CDA 24CDA1274310(SB), NIH NHLBI R01HL160138(SU), NIH/NHLBI R01HL127342, R01HL111656, and R01HL158108 (RFM)

Experimental design, manuscript preparation, AO- Assisted with design of immunohistochemistry experiments, RM- Experimental design, manuscript preparation, and correspondence.

Abstract

Introduction: Pulmonary arterial hypertension (PAH) is associated with neurocognitive deficits and abnormal brain MRI. Little is known about the mechanisms underlying these clinical observations. TDP-43 is a proteinopathy associated with frontotemporal lobar degeneration (FTLD), Alzheimer's Disease, and Amyotrophic Lateral Sclerosis (ALS). In this study, we hypothesize PAH will result in gliosis, reduced neuronal density, and increased TDP-43 mislocalization. **Methods:** Sprague Dawley rats were randomly assigned to receive Vehicle (DMSO) Monocrotaline, or Sugen/Hypoxia to induce PH. Right heart catheterization was used to confirm PAH. Brain tissue was fixed and probed for microglia (Iba1), astrocytes (GFAP), neurons (NeuN), and TDP-43. Human PH vs control brain tissue was also probed for NeuN and TDP-43. **Results and Conclusions:** We identify an increase in microglia and astrocyte density in the frontal cortex along with reduced neuronal density and neuronal TDP-43 mislocalization in rat models of PH. In addition, human PH frontal cortex demonstrated neuronal TDP-43 mislocalization. This is the first evidence of TDP-43 proteinopathy in PH.

Keywords

Pulmonary Hypertension; Neurodegeneration; Neuroinflammation; TDP-43;

43 **Abbreviations**

44 Pulmonary Hypertension (PH)

45 TAR DNA-binding protein 43 (TDP-43)

46 Amyotrophic Lateral Sclerosis (ALS)

47 Frontotemporal Lobar Degeneration (FTLD)

48 Pulmonary artery endothelial cell (PAEC)

49 Central nervous system (CNS)

50 Dimethyl sulfoxide (DMSO)

51 Monocrotaline (MCT)

52 Right Ventricular Systolic Pressure (RVP)

53 Phosphate Buffered Saline-Triton X (PBST)

54 Ionized calcium-binding adaptor molecule 1 (Iba1)

55 Glial Fibrillary Acidic Protein (GFAP)

56 Neuron-Specific Nuclear Protein (NeuN)

57 Polymerase Chain Reaction (PCR)

58 Sugen/Hypoxia (SuHx)

59

60 Differentially expressed genes (DEGs)

61

62 False discovery rate (FDR)

63 **Introduction**

64 Pulmonary hypertension (PH) is a severe condition, defined by an elevated mean pulmonary arterial
65 pressure exceeding 20 mmHg, and affects approximately 1% of the global population[1]. Clinical studies indicate
66 that patients with PH exhibit cognitive impairments, including challenges in executive function, memory,
67 calculation, and visuospatial abilities[2–4]. A small imaging study reveals a reduction in grey matter volume on
68 brain magnetic resonance imaging when compared to healthy age-matched control subjects, indicating
69 potential neuronal loss [5]. Research on the pathophysiological effects of PH on the central nervous system
70 remains limited. Animal studies have indicated increased concentrations of microglia and astrocytes in the
71 hypothalamus and thoracic spinal cord in subjects with PH compared to control groups, which may correlate
72 with the severity of PH[6,7]. The integration of clinical and animal data suggests the presence of
73 neuroinflammatory and neurodegenerative processes.

74 TAR DNA-binding protein 43 (TDP-43), a critical regulator of RNA metabolism, has been extensively
75 implicated in neurodegenerative disorders such as amyotrophic lateral sclerosis (ALS) and frontotemporal
76 lobar degeneration (FTLD)[8–10]. Pathological mislocalization and aggregation of TDP-43 disrupt RNA splicing,
77 translation, and intracellular transport—processes essential to both neuronal and endothelial cell function[11,12].
78 Recent data suggest a potential link between TDP-43 and inflammation, implicating it as a convergent node in
79 pulmonary hypertension (PH)-associated multi-organ dysfunction. Notably, pathologic extranuclear TDP-43
80 aggregation occurs under pro-inflammatory conditions such as stroke and traumatic brain injury[11,12]. The role of
81 TDP-43 in PH-associated neurodegeneration has not yet been explored.

82 In this study, we investigated the role of pulmonary hypertension (PH) in cortical neuroinflammation and
83 neurodegeneration through complementary methodologies. We characterized brain tissue from animal models
84 of PH to evaluate astrocyte, microglia, and neuronal densities, as well as TDP-43 proteinopathy. Additionally,
85 we examined neuronal density and TDP-43 proteinopathy in brain tissue samples from PH patients. Given the
86 emerging evidence linking TDP-43 to endothelial dysfunction, we conducted a secondary analysis of
87 pulmonary artery endothelial cell (PAEC) transcriptomic data to identify potential TDP-43-regulated genes.
88 While our studies on animal and human tissues concentrated on central nervous system (CNS) pathology,

these transcriptomic insights suggest a vascular component to the neuroinflammatory processes observed in PH. We hypothesize that PH induces cortical neuroinflammation, neurodegeneration, and TDP-43 proteinopathy.

Methods

Animal Models of Pulmonary Hypertension and Hemodynamic Measurements

All experimental procedures were sanctioned by the Institutional Animal Care and Use Committee at Indiana University. Following standard protocol as previously described[13], male and female Sprague Dawley rats (190-200 g) were procured from Charles River and randomly allocated to receive either Vehicle (Dimethyl sulfoxide (DMSO), intraperitoneal (ip) vehicle injection as a control), Monocrotaline (MCT; ip, 60 mg/kg of body weight), or Sugen (subcutaneously, 20 mg/kg body weight). Rats administered Sugen were housed in a 10% oxygen chamber for three weeks, followed by two weeks under normoxia conditions. At five weeks post-injection, the rats underwent open field testing, as previously described[14]. Briefly, the rats were placed in an open field maze, and measurements of distance traveled, time spent in the center, time at rest, and average ambulatory velocity were recorded using Any-maze software. Right Ventricular Systolic Pressure (RVP) was assessed via right heart catheterization employing a Millar pressure transducer catheter at the time of euthanasia. The Fulton index was calculated by measuring the ratio of the right ventricle weight to the sum of the weights of the left ventricle and septum (RV/(LV+S)). Brain tissue and plasma were collected at the time of euthanasia.

Rat Brain Tissue Immunofluorescence Staining

The brains were meticulously dissected along the intracerebral fissure, with one half snap-frozen in liquid nitrogen and stored at -80°C for subsequent RNA analyses. The remaining half was allocated for immunofluorescence studies and was fixed with 4% paraformaldehyde overnight, followed by a 24-hour treatment with 30% sucrose. The brains were then stored in optimal tissue cutting medium at -80°C until sectioning. Coronal sections were prepared at a thickness of 30 micrometers and preserved in cryoprotectant solution (FD NeuroTechnologies, Inch, Cat#PC102). The sections underwent heat-mediated antigen retrieval for 30 minutes at 80°C (Universal HEIR antigen retrieval reagent, Abcam#ab208572). Subsequently, the

115 sections were washed with 0.3% Phosphate Buffered Saline-Triton X-100 (PBST) and subjected to a 10-
116 minute treatment with 0.3% Hydrogen Peroxide block. Following additional washing, the sections were
117 incubated with 10% Donkey Serum (Abcam, #NC1697010) for 1 hour at room temperature. The sections were
118 then incubated overnight with primary antibodies (Supplemental Table 1). After the overnight incubation, the
119 sections were washed with PBST, blocked with 10% Donkey Serum, and incubated with secondary antibodies
120 (1:1000) for 2 hours. The sections were then washed with PBST and mounted on slides using ProLong Gold
121 Antifade Mountant with DNA Stain DAPI (Invitrogen, #P36931). Imaging was conducted using the Leica
122 Thunder System (20x magnification unless specified), and the images were analyzed using Imaris (Oxford
123 Instruments) to quantify cells positively expressing both DAPI and cell-specific marker.

124 **Rat Brain Quantitative Polymerase Chain Reaction (PCR)**

125 RNA was extracted from hemibrains utilizing the RNeasy Plus Mini Kit (Qiagen, # 74134) in accordance
126 with the manufacturer's protocol. The quality of the RNA was evaluated using the NanoDrop One.
127 Subsequently, RNA was transcribed into cDNA employing the High-Capacity cDNA Reverse Transcription Kit
128 (Applied Biosystems, # 4368814) with the Bio-rad T100 Thermal Cycler. Relative quantitative RT-PCR was
129 conducted using the Roche Lightcycler 480 and the PowerUP SYBR Green Master Mix chemistry (Applied
130 Biosystems, # A25742) to quantify cytokine gene expression. The primers used were as follows: *IL-6* (Forward
131 'TCCTACCCCAACTTCCAATGCTC', Reverse 'TTGGATGGTCTTGGTCCTTAGCC'), *IL-1β* (Forward
132 'CACCTCTCAAGCAGAGCACAG', Reverse 'GGGTTCCATGGTGAAGTCAAC'), *TNF-α* (Forward
133 'AAATGGGCTCCCTCTCATCAGTTC', Reverse 'TCTGCTTGGTGGTTTGCTACGAC'), and *Gapdh* (Forward
134 'CATCACTGCCACCCAGAAGACTG', Reverse 'ATGCCAGTGAGCTTCCCGTTCAG'). The fold change was
135 calculated using the $2^{-\Delta\Delta CT}$ method, with results normalized to *Gapdh*.

136 **Human Cortical Tissue Immunohistochemistry**

137 In accordance with 45 CFR 46, our study does not involve human subjects but used deidentified human
138 tissues provided by UCLA Pathology departmental honest broker, the UCLA Translational Pathology Core Lab
139 (IRB# 11-002504). Paraffin-embedded 5 micrometer thick human brain cortex sections (Control n=3, PH n=4)
140 were rehydrated, and antigen retrieval was performed by heat-induced epitope retrieval at pH 6 (C9999,

141 Sigma). Tissue sections were blocked for an hour at room temperature in PBS with 5% goat serum, 1% BSA,
142 0.1% Triton, 0.05% Tween, and 0.3 M glycine. Tissue sections were incubated overnight with primary
143 antibodies diluted 1:200 in PBS with 1% BSA and 0.5% Triton at 4°C. Secondary antibodies were incubated for
144 an hour at room temperature and diluted 1:1000 in PBS with 0.05% Tween. Sections were incubated with
145 ProLong™ Gold antifade mountant with DNA Stain DAPI and cover slips were applied. All images were
146 acquired using a confocal microscope (40x magnification) (Nikon). A total of 4-5 images were acquired from
147 each slide. Images were analyzed using Imaris (Oxford Instruments).

148 **Secondary Analysis of TDP-43-Regulated Genes in Pulmonary Artery Endothelial Cells**

149 Raw gene expression count data were procured from the NCBI Gene Expression Omnibus (GEO)
150 under accession number GSE243193, encompassing RNA-sequencing data from human pulmonary artery
151 endothelial cells (PAECs) isolated from patients with group 1 pulmonary hypertension (PH) (n=20) and controls
152 (n=3) [15]. Group 1 PH patients were selected as they more closely align with the animal models represented in
153 this study. The dataset was imported into R (version 4.2.0) and underwent preprocessing to eliminate genes
154 with missing or NA values across samples[16]. Following quality control, expression counts were converted into a
155 matrix. Samples were categorized as “PH” or “Control” based on their column names, and group labels were
156 encoded as a factor variable for subsequent differential expression analysis. Gene expression normalization
157 and differential analysis were conducted using the edgeR and limma packages[17,18]. Expression counts were
158 filtered using filterByExpr() to retain genes with adequate counts across samples. Library sizes were
159 normalized using the trimmed mean of M-values (TMM), and log2-transformed counts per million (CPM) were
160 calculated via voom to model the mean-variance relationship[19]. Linear modeling was executed using lmFit(),
161 followed by empirical Bayes moderation using eBayes() to enhance variance estimation. Differentially
162 expressed genes (DEGs) were identified based on false discovery rate (FDR)-adjusted p-values < 0.05. Gene
163 annotation was performed using the org.Hs.eg.db Bioconductor package to map ENTREZ identifiers to gene
164 symbols and gene names[20]. To evaluate the enrichment of TDP-43 regulatory activity in PH-associated gene
165 expression changes, a curated list of TDP-43 RNA targets was obtained from POSTAR3 CLIP-seq datasets[21].
166 POSTAR-3 utilizes data from the ENCODE project which identified TDP-43 targets under baseline conditions.
167 Although these targets were identified in non-diseased immortalized cells, they provide a reference map of

168 physiologic TDP-43 binding sites, which may be dysregulated or lost in disease-specific contexts such as
169 nuclear exclusion[22].The overlap between differentially expressed genes (FDR < 0.05) and TDP-43 targets was
170 calculated. A Fisher's exact test was conducted to assess whether TDP-43 targets were statistically
171 overrepresented among DEGs compared to the background set of all expressed genes. A 2×2 contingency
172 table was constructed with counts of genes categorized as TDP-43 target vs. non-target and DEG vs. non-
173 DEG. The resulting odds ratio and p-value were utilized to determine enrichment significance. A volcano plot
174 was generated using ggplot2, with upregulated and downregulated genes highlighted[23]. ChatGPT was used for
175 code debugging.

176 **Statistical Analysis**

177 Statistical analyses were performed utilizing GraphPad Prism (version 8.4.3; GraphPad Software) and R
178 (version 4.2.0), as delineated in the preceding section. To compare experimental groups (e.g., SuHx vs. Vehicle
179 and MCT vs. Vehicle), an unpaired two-tailed Student's t-test was employed. Linear regression analysis was
180 conducted to assess correlations between variables. Pearson's correlation coefficient (r) and the coefficient of
181 determination (R^2) were calculated and reported. Data are presented as mean ± standard error of the mean
182 (SEM) unless otherwise specified. A p-value < 0.05 was considered indicative of statistical significance.

183 **Results**

184 **SuHx-Induced Pulmonary Hypertension is Associated with Elevated RVP and Hypertrophy**

185 Sugen/hypoxia (SuHx) and monocrotaline (MCT) are established models for the study of pulmonary
186 hypertension (PH) and were employed to induce PH in rats[24]. The presence of pulmonary hypertension was
187 confirmed through measurements of right ventricular pressure (RVP) and right ventricular hypertrophy (Fulton
188 Index). The SuHx model (n=6) elicited a pronounced PH phenotype, evidenced by a significant increase in RVP
189 (mean difference of 52.33 ± 11.84 mmHg compared to vehicle controls, n=6; p=0.0013) and the Fulton index
190 (mean difference of 0.2428 ± 0.03486, p<0.0001) (**Figure 1**). Conversely, the MCT model (n=6) demonstrated
191 a trend towards increased RVP (mean difference of 17.33 ± 6.98 mmHg versus controls, p=0.0522) and a modest
192 yet statistically significant increase in the Fulton Index (mean difference of 0.09815 ± 0.03066 versus controls,
193 p=0.0198) (**Supplemental Figure 1**). Although this study was not designed or powered to assess sex differences

194 (n=3 males and n=3 females per group), exploratory analysis indicated a sex-dependent effect in both models.
195 In SuHx-treated rats, males exhibited higher RVP (mean: 102.67 mmHg) and Fulton Index (mean: 0.53)
196 compared to females (mean RVP: 52 mmHg; mean Fulton index: 0.41). A similar pattern was observed in MCT-
197 treated animals, with males showing higher RVP (mean: 56 mmHg) and Fulton Index (mean: 0.36) compared to
198 females (mean RVP of 27 mmHg; mean Fulton index of 0.28). These findings align with existing literature on sex
199 differences in experimental PH and highlight the necessity of considering sex as a biological variable in preclinical
200 studies[25]. No statistically significant sex differences were observed in any of the subsequent measurements.
201 This suggests a need for further exploration of the impact of sex as a biological variable in neuroinflammation in
202 PH. Due to the relatively mild phenotype induced by MCT in our study (likely due to the modest effect on female
203 mice), all MCT-associated findings, including cardiovascular and central nervous system assessments, are
204 included in the supplemental materials.

205 **No Behavioral Abnormalities are Observed in Open Field Testing**

206 Open field testing (OFT) is widely used to assess sickness behavior, locomotor activity, and anxiety-like
207 behavior in rodent models of systemic disease, including those of sepsis-associated encephalopathy, heart
208 failure, and frontotemporal lobar degeneration[26–28]. In this study, OFT was employed to evaluate whether PH
209 was associated with changes in exploratory behavior or activity levels. SuHx-treated rats showed no significant
210 differences in total distance traveled, time spent in the center of the arena, time spent at rest, or average
211 ambulatory velocity compared to vehicle-treated controls (**Figure 2**). Similarly, no statistically significant
212 differences were observed between MCT-treated rats and controls (**Supplemental Figure 2**). OFT data did not
213 correlate significantly with RVP or Fulton in either model (data not shown).
214

215 **Experimental PH Induces Neuroinflammation**

216 Neuroinflammation is recognized as an early and critical risk factor for neurodegeneration[29,30]. In this
217 study, we measured cortical density of microglia and astrocytes in two rodent models of PH. In SuHx-treated
218 rats, microglial density was significantly increased ($3.875 \times 10^{-5} \pm 1.504 \times 10^{-5}$ cells/μm^2 compared to vehicle-
219 treated controls ($n = 6$; $p = 0.0276$). Astrocyte density was also elevated in SuHx animals ($4.487 \times 10^{-5} \pm 1.806$
220 $\times 10^{-5}$ cells/μm^2, $p = 0.0323$) (**Figure 3**). Notably, neither microglia nor astrocytic density correlated with RVP

221 or Fulton Index in the SuHx group (data not shown). In the MCT-treated rats, a significant increase in microglial
222 density (0.2320 ± 0.009541 cells/μm^2) compared to vehicle-treated controls (n = 6; p <0.0001) was observed
223 (**Supplemental Figure 3**). Similarly, astrocyte density was elevated in MCT-treated animals relative to control
224 ($4.822 \times 10^{-5} \pm 1.309 \times 10^{-5}$ cells/μm^2, p= 0.0043) (**Supplemental Figure 3**). Unlike the SuHx-treated animals,
225 cortical microglia density positively correlated with the RVP (r= 0.7670, 95% CI: 0.3449 to 0.9311, p=0.0036)
226 and Fulton Index (r= 0.7990, 95% CI: 0.4156 to 0.9413, p=0.0018). Despite increased glial density, there was
227 no increase in cortical expression of pro-inflammatory cytokines—including IL-1β, TNF-α, or IL-6 mRNA—
228 between SuHx- or MCT-treated animals and their respective controls, with SuHx data presented in **Figure 4**
229 and MCT data presented in **Supplemental Figure 4.**
230

231 **Experimental PH Induces Neuronal Loss and TDP-43 Proteinopathy**

232 Neurodegeneration is characterized by the progressive loss of neurons and associated structural and
233 functional decline[31]. A hallmark of several neurodegenerative diseases is TDP-43 proteinopathy, defined by the
234 pathological mislocalization of TAR DNA-binding protein 43 (TDP-43) from the nucleus to the cytoplasm. While
235 traditionally linked to conditions such as amyotrophic lateral sclerosis (ALS) and frontotemporal lobar
236 degeneration (FTLD), TDP-43 pathology has also been identified in proinflammatory states, including traumatic
237 brain injury and stroke[8,9,11,12]. In the SuHx model, we observed a significant reduction in cortical neuronal
238 density compared to vehicle controls (n = 6), with a mean difference of $-0.0001113 \pm 2.937 \times 10^{-5}$ cells/μm^2
239 (p = 0.0035). SuHx-treated animals also exhibited a significant increase in neuronal extranuclear TDP-43, with
240 a mean difference of 0.2592 ± 0.0432 (p < 0.0001). Linear regression analysis revealed that right ventricular
241 pressure (RVP) significantly predicted neuronal density (R^2 = 0.5825, p = 0.0039) and the proportion of
242 neurons with extranuclear TDP-43 (R^2 = 0.4029, p = 0.0266) (**Figure 5**). Similarly, the Fulton index strongly
243 predicted both neuronal density (R^2 = 0.6898, p = 0.0008) and extranuclear TDP-43 burden (R^2 = 0.6001, p =
244 0.0031) (data not shown).

245 In contrast, MCT-treated animals showed no significant change in neuronal density relative to controls
246 (n = 6). However, MCT treatment was associated with a significant increase in neuronal extranuclear TDP-43

247 (mean difference: 0.2553 ± 0.0762, $p = 0.0194$) (**Supplemental Figure 5**). Notably, in the MCT group, neither
248 RVP nor Fulton index correlated with neuronal density or extranuclear TDP-43.

249 **Clinical PH Induces Cortical TDP-43 Proteinopathy**

250 To investigate the potential impact of pulmonary hypertension (PH) on neurodegeneration and TDP-43
251 proteinopathy in humans, we analyzed postmortem cortical brain tissue from individuals with PH ($n = 4$) and
252 non-PH controls ($n = 3$). Quantitative analysis revealed no significant difference in cortical neuronal
253 density between the two groups. However, neuronal extranuclear TDP-43 was significantly increased in PH
254 subjects compared to controls, with a mean difference of 46.27 ± 12.96 ($p = 0.0230$) (**Figure 6**). Demographics
255 available in supplemental table 2.
256

257 **PH Disproportionately Affects Expression of TDP-43 Regulated Genes in Pulmonary Artery Endothelial**
258 **Cells (PAECs)**

259 Emerging evidence suggests that TDP-43 is essential for endothelial cell function and RNA
260 homeostasis[10,32]. This may represent a critical mechanistic link between TDP-43 proteinopathy and pulmonary
261 hypertension (PH), implicating endothelial dysregulation as a contributor to the neurodegenerative processes
262 observed in PH. To explore this hypothesis, we performed a secondary analysis of single-cell RNA sequencing
263 data (GSE243193) from pulmonary artery endothelial cells[15]. We identified TDP-43 target transcripts using
264 POSTAR3 CLIP-seq data and applied Fisher's exact test to determine whether PH disproportionately
265 dysregulates TDP-43–regulated genes[21]. Top downregulated genes were manually annotated using
266 GeneCards[33]. This analysis revealed a significant overrepresentation of TDP-43–associated transcripts among
267 the downregulated genes in PH (Fisher's exact test: $p < 2.2 \times 10^{-16}$, OR: 0.193, 95% CI: 0.139-0.269),
268 suggesting selective vulnerability of this RNA-regulatory pathway. Notably, many of the top downregulated
269 TDP-43 targets are involved in RNA processing (EIF4A1, HNRNPH2), vesicular trafficking (SNX15, CHMP3,
270 RAB4B), and inflammation (MIF) (**Figure 7**).
271

272 **Discussion**

273 Pulmonary hypertension (PH) is increasingly acknowledged as a systemic condition that affects not
274 only the pulmonary vasculature and the right ventricle but also encompasses cognitive, affective, and
275 neuroinflammatory consequences[2–4,7]. While prior clinical studies have documented neurocognitive symptoms
276 in PH patients, the underlying pathophysiology linking pulmonary vascular disease to central nervous system
277 (CNS) injury has remained poorly defined. Although previous clinical studies have documented neurocognitive
278 symptoms in patients with PH, the pathophysiological mechanisms linking pulmonary vascular disease to
279 central nervous system (CNS) injury remain inadequately defined. In this study, we present preclinical and
280 translational evidence suggesting that gliosis and TDP-43 proteinopathy are contributing factors to the
281 development of neurodegeneration in PH.

282 Our findings elucidate significant distinctions between the MCT and SuHx models of pulmonary
283 hypertension (PH). Both models indicate a sex-related disparity in PH and vascular remodeling, aligning with
284 existing literature[34]. As previously reported, the MCT induced a less severe PH phenotype in females, which
285 resulted in right ventricular hypertrophy without elevated right ventricular pressure[34]. Notably, there are
286 differences in central nervous system (CNS) findings between these models. Both models exhibit gliosis and
287 TDP-43 proteinopathy; however, the more severe SuHx model also shows reduced neuronal density. The
288 severity of PH correlates with TDP-43 proteinopathy and neuronal loss in the SuHx model, whereas in the
289 MCT model, it predicts microglial activation. This suggests that CNS findings may occur on a spectrum, with
290 milder forms of PH inducing neuroinflammation, while more severe PH leads to neuronal loss. The SuHx and
291 MCT models of pulmonary hypertension exhibit distinct pathological mechanisms, which may have implications
292 for extrapulmonary involvement, including the brain. The SuHx model combines VEGF receptor inhibition with
293 chronic hypoxia to induce severe, angio-obliterative pulmonary vascular remodeling. This model simulates a
294 progressive, endothelial-driven vasculopathy, which may potentially exacerbate blood-brain barrier (BBB)
295 dysfunction and cerebral microvascular injury.[35]. Monocrotaline, in contrast, induces pulmonary hypertension
296 through a singular, systemic endothelial toxin that preferentially damages the pulmonary vasculature via
297 hepatic metabolism. Although effective in promoting vascular remodeling and right ventricular hypertrophy,
298 monocrotaline is associated with systemic toxicity, including hepatic and renal injury, and may exert more
299 variable effects on the cerebral vasculature. [35]. Given the critical role of hypoxia in influencing neurovascular

300 integrity and mitochondrial metabolism, the Sugen hypoxia model may more accurately represent brain-
301 relevant systemic stressors, such as chronic cerebral hypoxemia. In contrast, the MCT model may complicate
302 interpretation due to its extensive systemic toxicities. Our limited clinical data revealed an increase in TDP-43
303 proteinopathy among patients with PH compared to control subjects.

304 TDP-43, a nuclear RNA-binding protein with established roles in neurodegenerative diseases such as
305 ALS and frontotemporal dementia, has recently been implicated in vascular and endothelial cell biology[10,32] In
306 these studies, the depletion of endothelial TDP-43 resulted in diminished expression of tight junction proteins,
307 such as claudin-5, heightened permeability, and the activation of microglia and astrocytes.[36,37]. Although our
308 studies on animal and human tissues concentrated on neuronal pathology, we hypothesized that endothelial
309 dysfunction might contribute to PH-associated neuroinflammation through TDP-43–mediated post-
310 transcriptional dysregulation. To investigate this hypothesis, we conducted a secondary analysis of single-cell
311 RNA sequencing data from pulmonary artery endothelial cells (GSE243193), focusing on transcripts known to
312 be regulated by TDP-43 using POSTAR3 CLIP-seq data[15,21]. This analysis demonstrated that PH
313 disproportionately downregulates TDP-43 target genes in endothelial cells, with key affected transcripts
314 involved in RNA metabolism (EIF4A1, HNRNPH2), vesicular trafficking (CHMP3, SNX15, RAB4B),
315 mitochondrial homeostasis (MRPS24, PLSCR3), and inflammatory signaling (MIF)[33]. These findings support a
316 model in which TDP-43–associated transcriptomic dysregulation may impair endothelial function in PH,
317 potentially contributing to downstream neuroinflammation and blood-brain barrier vulnerability. While we did
318 not directly assess blood-brain barrier (BBB) integrity in this study, the observed gene expression changes
319 implicate pathways known to affect endothelial stability. Importantly, these data do not suggest that TDP-43
320 dysfunction is merely a consequence of chronic hypoxia or right heart failure. Rather, they propose that TDP-
321 43 dysregulation is a shared molecular feature of both pulmonary vascular and neurologic injury in PH. This
322 hypothesis aligns with recent literature demonstrating the role of TDP-43 in oxidative stress responses and
323 RNA transport in both neurons and endothelial cells[9,10,32,38].

324 Our study has several limitations. Firstly, although the neuroinflammatory and degenerative alterations
325 were pronounced in both animal and human PH brain tissue, we did not directly demonstrate functional

326 impairments, such as behavioral or cognitive deficits. Further work is needed to phenotype cognitive
327 impairment in PH animal models. While an open field test is beneficial for identifying locomotion, anxiety, and
328 sickness behavior in animal models, it may not effectively simulate the loss of executive function observed in
329 frontotemporal lobar degeneration (FTLD), which is also challenging to differentiate from motor dysfunction in a
330 clinical context [39]. Next, quantitative PCR analysis did not reveal a significant difference in proinflammatory
331 cytokine mRNA levels, indicating that further investigation is required to determine the timing of
332 neuroinflammation in relation to the onset of pulmonary hypertension. An additional limitation is the use of a
333 limited data tissue biobank utilized to investigate TDP-43 in PH patients. This dataset does not include
334 information regarding PH duration or severity which could influence the results. In addition, while our
335 transcriptomic analysis indicates endothelial contributions to the TDP-43 signature, further research is
336 necessary to validate these targets at the protein level and to assess causality using endothelial-specific TDP-
337 43 models. Lastly, our study was not powered to assess sex as a biological variable which may be an
338 important direction for future studies. In sum, the temporal sequence of neuroinflammation, TDP-43
339 mislocalization, endothelial dysfunction, and CNS injury remains to be elucidated.

340 Despite these limitations, our findings establish a foundational basis for a novel conceptual model of PH
341 as a multisystem disorder characterized by mechanistic links to RNA dysregulation and neurodegeneration.
342 Targeting TDP-43 or its downstream pathways may present therapeutic opportunities to mitigate both vascular
343 and neurological complications in this population. Future research focused on elucidating the cell-specific roles
344 of TDP-43 within the lung-brain axis may yield further insights into the systemic nature of pulmonary vascular
345 disease.

346 **Conclusion:**

347 This study identifies TDP-43 dysregulation as a potential mechanistic link between pulmonary
348 hypertension and central nervous system injury. Through the integration of animal models, human brain tissue,
349 and endothelial transcriptomic analysis, we demonstrate that PH is associated with neuroinflammatory and
350 neurodegenerative changes, alongside selective downregulation of TDP-43–regulated genes in pulmonary
351 artery endothelial cells. These findings support a novel model in which TDP-43 contributes to multisystem

dysfunction in PH, bridging vascular and neurologic pathology. Elucidating the role of TDP-43 across organ systems may open new avenues for targeted therapies aimed at mitigating both cardiopulmonary and cognitive complications of PH.

Acknowledgements: This work was supported by the Behavioral Phenotyping Core (BPC) at the Indiana University School of Medicine.

References

1. Hoeper MM, Humbert M, Souza R, et al. A global view of pulmonary hypertension. *Lancet Respir Med*. 2016;4(4):306-322. doi:10.1016/S2213-2600(15)00543-3

2. Heller S, See C, Singh I, Fredericks CA. Cognitive impairment in pulmonary arterial hypertension. *Ann Clin Transl Neurol*. 2023;10(10):1899-1903. doi:10.1002/acn3.51867

3. White J, Hopkins RO, Glissmeyer EW, Kitterman N, Elliott CG. Cognitive, emotional, and quality of life outcomes in patients with pulmonary arterial hypertension. *Respir Res*. 2006;7(1):55. doi:10.1186/1465-9921-7-55

4. Yuan P, Li J, Liu J, et al. Cognitive Dysfunction in Patients with Pulmonary Hypertension. *Am J Respir Crit Care Med*. 206(10):1289-1293. doi:10.1164/rccm.202204-0726LE

5. Roy B, Vacas S, Ehlert L, McCloy K, Saggar R, Kumar R. Brain Structural Changes in Patients with Pulmonary Arterial Hypertension. *J Neuroimaging Off J Am Soc Neuroimaging*. 2021;31(3):524-531. doi:10.1111/jon.12840

6. Sharma RK, Oliveira AC, Kim S, et al. Involvement of Neuroinflammation in the Pathogenesis of Monocrotaline-Induced Pulmonary Hypertension. *Hypertens Dallas Tex 1979*. 2018;71(6):1156-1163. doi:10.1161/HYPERTENSIONAHA.118.10934

7. Razee A, Banerjee S, Hong J, et al. Thoracic Spinal Cord Neuroinflammation as a Novel Therapeutic Target in Pulmonary Hypertension. *Hypertension*. 2023;80(6):1297-1310. doi:10.1161/HYPERTENSIONAHA.122.20782

8. Jo M, Lee S, Jeon YM, Kim S, Kwon Y, Kim HJ. The role of TDP-43 propagation in neurodegenerative diseases: integrating insights from clinical and experimental studies. *Exp Mol Med*. 2020;52(10):1652-1662. doi:10.1038/s12276-020-00513-7

9. Zuo X, Zhou J, Li Y, et al. TDP-43 aggregation induced by oxidative stress causes global mitochondrial imbalance in ALS. *Nat Struct Mol Biol*. 2021;28(2):132-142. doi:10.1038/s41594-020-00537-7

10. Cheemala A, Kimble AL, Burrage EN, et al. Amyotrophic lateral sclerosis and frontotemporal dementia mutation reduces endothelial TDP-43 and causes blood-brain barrier defects. *Sci Adv*. 2025;11(16):eads0505. doi:10.1126/sciadv.ads0505

11. Thammisetty SS, Pedragosa J, Weng YC, Calon F, Planas A, Kriz J. Age-related deregulation of TDP-43 after stroke enhances NF-κB-mediated inflammation and neuronal damage. *J Neuroinflammation*. 2018;15(1):312. doi:10.1186/s12974-018-1350-y

12. Bjorklund GR, Wong J, Brafman D, Bowser R, Stabenfeldt SE. Traumatic brain injury induces TDP-43 mislocalization and neurodegenerative effects in tissue distal to the primary injury site in a non-transgenic mouse. *Acta Neuropathol Commun*. 2023;11(1):137. doi:10.1186/s40478-023-01625-7

13. Chen J, Lockett A, Zhao S, et al. Sphingosine Kinase 1 Deficiency in Smooth Muscle Cells Protects against Hypoxia-Mediated Pulmonary Hypertension via YAP1 Signaling. *Int J Mol Sci*. 2022;23(23):14516. doi:10.3390/ijms232314516

14. Seibenhener ML, Wooten MC. Use of the Open Field Maze to Measure Locomotor and Anxiety-like Behavior in Mice. *J Vis Exp JoVE*. 2015;(96):52434. doi:10.3791/52434

15. Singh N, Eickhoff C, Garcia-Agundez A, et al. Transcriptional profiles of pulmonary artery endothelial cells in pulmonary hypertension. *Sci Rep*. 2023;13(1):22534. doi:10.1038/s41598-023-48077-6

16. R: The R Project for Statistical Computing. Accessed June 30, 2025. https://www.r-project.org/

17. Robinson MD, McCarthy DJ, Smyth GK. edgeR: a Bioconductor package for differential expression analysis of digital gene expression data. *Bioinformatics*. 2010;26(1):139-140. doi:10.1093/bioinformatics/btp616

18. Ritchie ME, Phipson B, Wu D, et al. limma powers differential expression analyses for RNA-sequencing and microarray studies. *Nucleic Acids Res*. 2015;43(7):e47. doi:10.1093/nar/gkv007

19. Law CW, Chen Y, Shi W, Smyth GK. voom: precision weights unlock linear model analysis tools for RNA-seq read counts. *Genome Biol*. 2014;15(2):R29. doi:10.1186/gb-2014-15-2-r29

20. org.Hs.eg.db. Bioconductor. Accessed June 30, 2025. http://bioconductor.org/packages/org.Hs.eg.db/

21. Zhao W, Zhang S, Zhu Y, et al. POSTAR3: an updated platform for exploring post-transcriptional regulation coordinated by RNA-binding proteins. *Nucleic Acids Res*. 2022;50(D1):D287-D294. doi:10.1093/nar/gkab702

22. Van Nostrand EL, Pratt GA, Yee BA, et al. Principles of RNA processing from analysis of enhanced CLIP maps for 150 RNA binding proteins. *Genome Biol*. 2020;21(1):90. doi:10.1186/s13059-020-01982-9

23. Wickham H. *Ggplot2: Elegant Graphics for Data Analysis*. Springer; 2009. doi:10.1007/978-0-387-98141-3

24. Boucherat O, Agrawal V, Lawrie A, Bonnet S. The Latest in Animal Models of Pulmonary Hypertension and Right Ventricular Failure. *Circ Res*. 2022;130(9):1466-1486. doi:10.1161/CIRCRESAHA.121.319971

25. Bal E, Ilgin S, Atli O, Ergun B, Sirmagul B. The effects of gender difference on monocrotaline-induced pulmonary hypertension in rats. *Hum Exp Toxicol*. 2013;32(7):766-774. doi:10.1177/0960327113477874

26. Swiergiel AH, Dunn AJ. Effects of Interleukin-1β and Lipopolysaccharide on Behavior of Mice in the Elevated Plus-Maze and Open Field Tests. *Pharmacol Biochem Behav*. 2007;86(4):651-659. doi:10.1016/j.pbb.2007.02.010

27. Dridi H, Liu Y, Reiken S, et al. Heart failure-induced cognitive dysfunction is mediated by intracellular Ca2+ leak through ryanodine receptor type 2. *Nat Neurosci*. 2023;26(8):1365-1378. doi:10.1038/s41593-023-01377-6

28. Frew J, Nygaard HB. Neuropathological and behavioral characterization of aged Grn R493X progranulin-deficient frontotemporal dementia knockin mice. *Acta Neuropathol Commun*. 2021;9:57. doi:10.1186/s40478-021-01158-x

29. Zhang W, Xiao D, Mao Q, Xia H. Role of neuroinflammation in neurodegeneration development. *Signal Transduct Target Ther*. 2023;8(1):1-32. doi:10.1038/s41392-023-01486-5

30. Kempuraj D, Thangavel R, Natteru P, et al. Neuroinflammation Induces Neurodegeneration. *J Neurol Neurosurg Spine*. 2016;1(1):1003.

31. Przedborski S, Vila M, Jackson-Lewis V. Series Introduction: Neurodegeneration: What is it and where are we? *J Clin Invest*. 2003;111(1):3-10. doi:10.1172/JCI17522

32. Arribas V, Onetti Y, Ramiro-Pareta M, et al. Endothelial TDP-43 controls sprouting angiogenesis and vascular barrier integrity, and its deletion triggers neuroinflammation. *JCI Insight*. 2024;9(5). doi:10.1172/jci.insight.177819

33. GeneCards - Human Genes | Gene Database | Gene Search. Accessed June 30, 2025. https://www.genecards.org/

459 34. Bal E, Ilgin S, Atli O, Ergun B, Sirmagul B. The effects of gender difference on monocrotaline-induced
460 pulmonary hypertension in rats. *Hum Exp Toxicol*. 2013;32(7):766-774. doi:10.1177/0960327113477874

461 35. Wu XH, Ma JL, Ding D, Ma YJ, Wei YP, Jing ZC. Experimental animal models of pulmonary hypertension:
462 Development and challenges. *Anim Models Exp Med*. 2022;5(3):207-216. doi:10.1002/ame2.12220

463 36. Cheemala A, Kimble AL, Tyburski JD, et al. Loss of Endothelial TDP-43 Leads to Blood Brain Barrier
464 Defects in Mouse Models of Amyotrophic Lateral Sclerosis and Frontotemporal Dementia. *bioRxiv*.
465 Published online December 14, 2023:2023.12.13.571184. doi:10.1101/2023.12.13.571184

466 37. Arribas V, Onetti Y, Ramiro-Pareta M, et al. Endothelial TDP-43 controls sprouting angiogenesis and
467 vascular barrier integrity, and its deletion triggers neuroinflammation. *JCI Insight*. 2024;9(5).
468 doi:10.1172/jci.insight.177819

469 38. Colombrita C, Zennaro E, Fallini C, et al. TDP-43 is recruited to stress granules in conditions of oxidative
470 insult. *J Neurochem*. 2009;111(4):1051-1061. doi:10.1111/j.1471-4159.2009.06383.x

471 39. Huey ED, Goveia EN, Paviol S, et al. Executive dysfunction in frontotemporal dementia and corticobasal
472 syndrome. *Neurology*. 2009;72(5):453-459. doi:10.1212/01.wnl.0000341781.39164.26

473

474

475 **Figures**

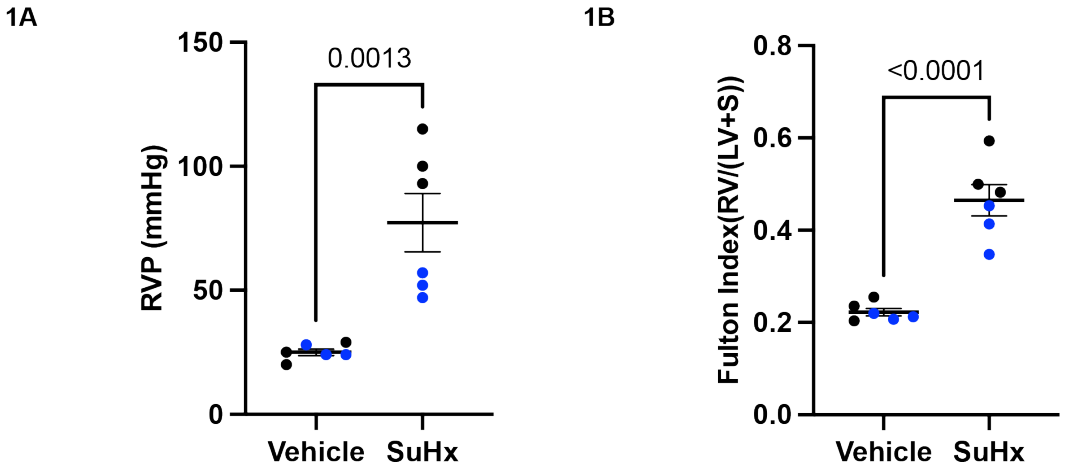

Figure 1. Sugen-hypoxia induces pulmonary hypertension and vascular remodeling. Rats treated with Sugen-hypoxia (SuHx; n = 6) exhibit increased right ventricular pressure (RVP), with a mean difference of 52.33 ± 11.84 mmHg compared to vehicle controls (n = 6; p = 0.0013) (**1A**). SuHx-treated rats also demonstrate right ventricular hypertrophy, with a mean Fulton Index difference of 0.2428 ± 0.03486 compared to controls (p < 0.0001) (**1B**). Data analyzed using a two-tailed unpaired t-test and are presented as mean ± SEM. Female animals are depicted in blue.

476

477

478

479

480

481

482

483

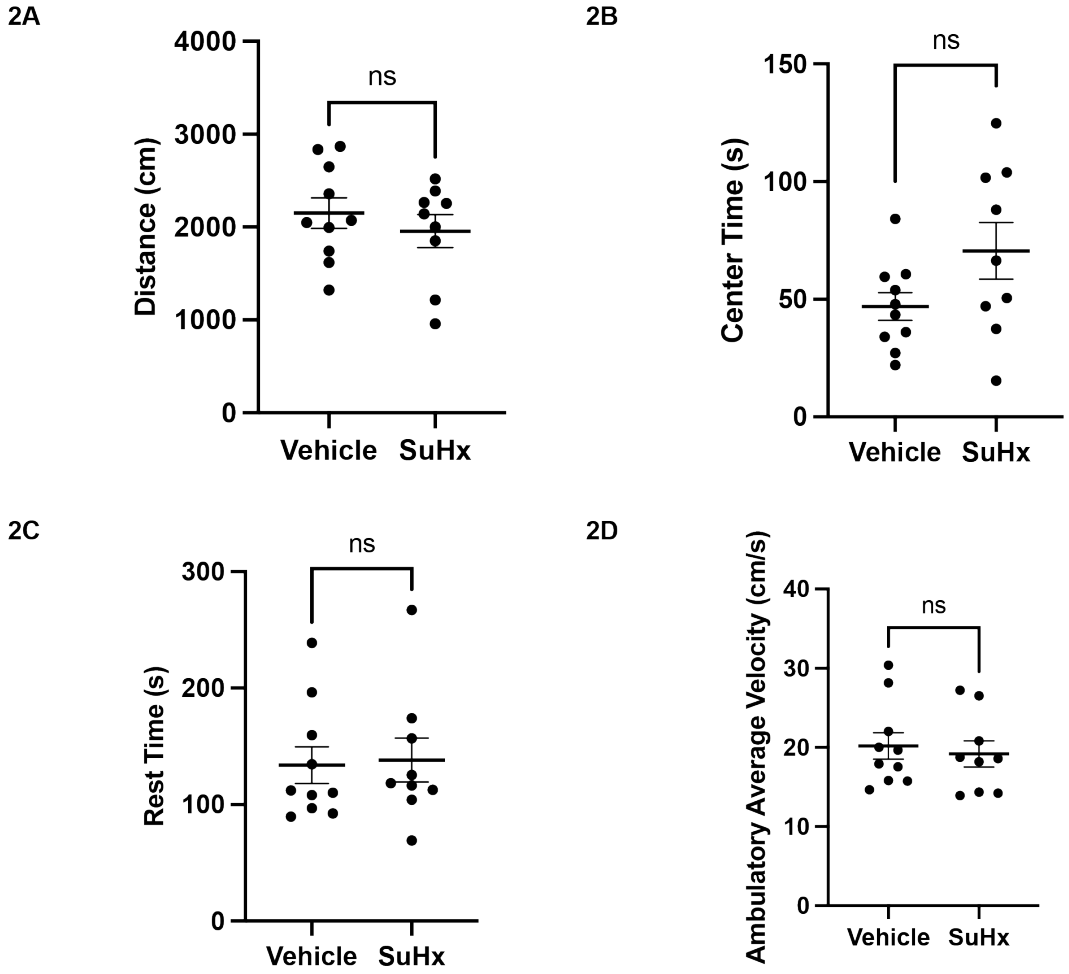

Figure 2. Sugen hypoxia does not induce sickness behavior in rats undergoing open field test. Rats exposed to Sugen hypoxia (SuHx, n = 9) did not exhibit significant differences in behavioral parameters compared to vehicle-treated controls (n = 10). Specifically, there were no significant changes in total distance traveled (**2A**), time spent in the center of the open field test (**2B**), time spent at rest (**2C**), or average ambulatory velocity (**2D**). Data were analyzed using an unpaired two-tailed t-test and are presented as mean ± SEM.

484

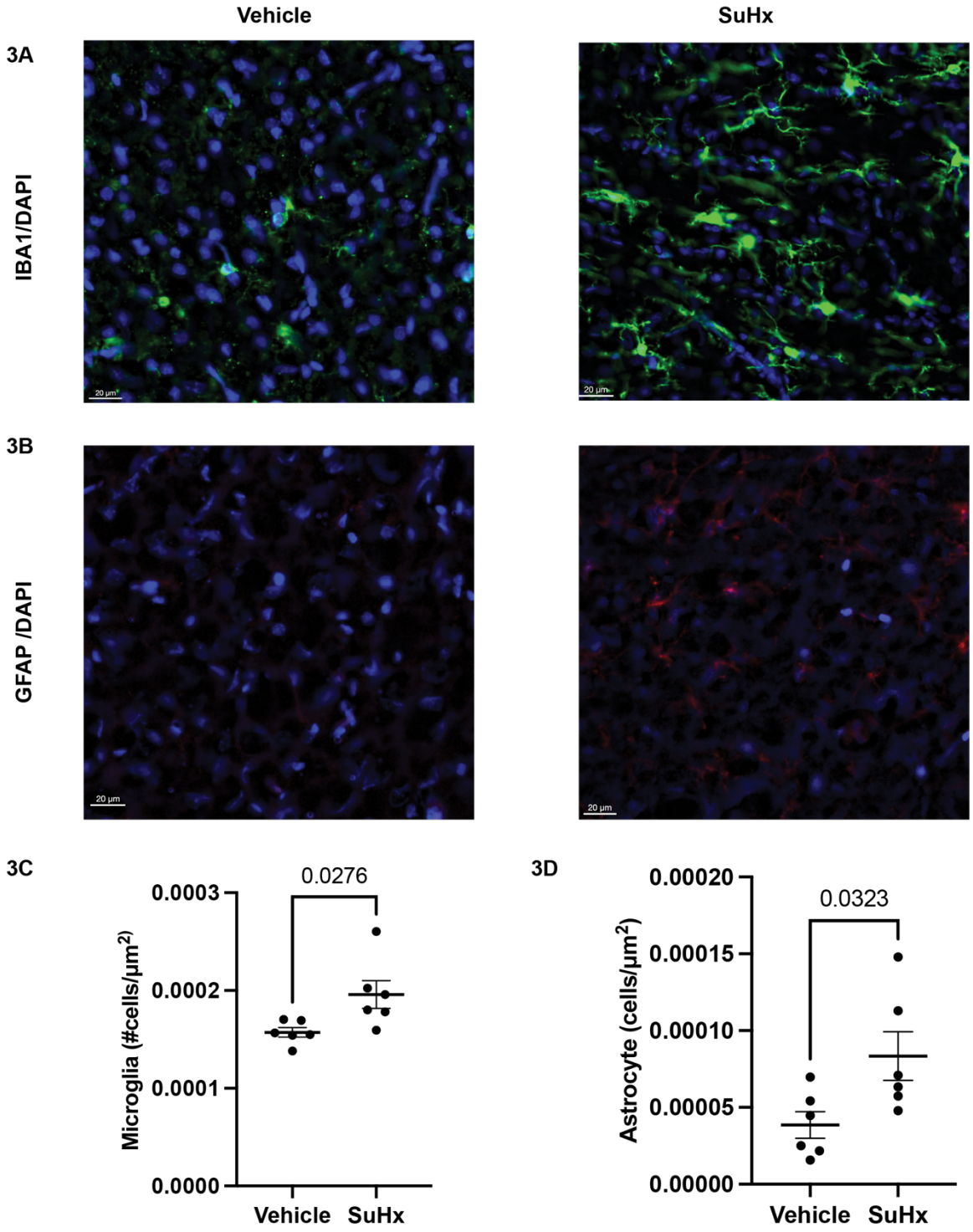

Figure 3. Sugen hypoxia increases cortical gliosis. Representative immunofluorescence images of frontal cortex microglia (IBA1/DAPI) (**3A**) and astrocytes (GFAP/DAPI) (**3B**) in rats exposed to sugen/hypoxia (SuHx) or vehicle. SuHx-treated rats (n = 6) exhibited a significantly increased microglial density ($3.875 \times 10^{-5} \pm 1.504 \times 10^{-5}$) compared to vehicle-treated controls (n = 6; p = 0.0276) (**3C**). Similarly, astrocyte density was elevated in SuHx-treated animals ($4.487 \times 10^{-5} \pm 1.806 \times 10^{-5}$) relative to controls (p = 0.0323) (**3D**). Data are presented as mean ± SEM and were analyzed using a two-tailed unpaired t-test.

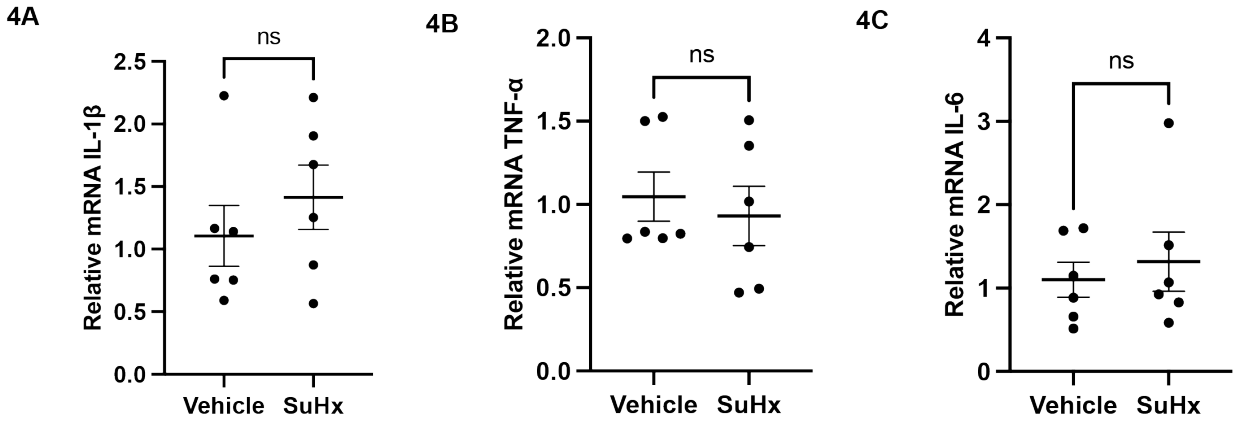

Figure 4. Sugen/hypoxia does not increase cortical cytokine expression. Quantitative PCR analysis of cortical cytokine mRNA expression in rats treated with sugen/hypoxia (SuHx; n = 6) or vehicle (n = 6) revealed no significant differences in IL-1β (**4A**), TNF-α (**4B**), or IL-6 (**4C**) transcript levels. Data are presented as mean ± SEM and were analyzed using a two-tailed unpaired t-test.

486

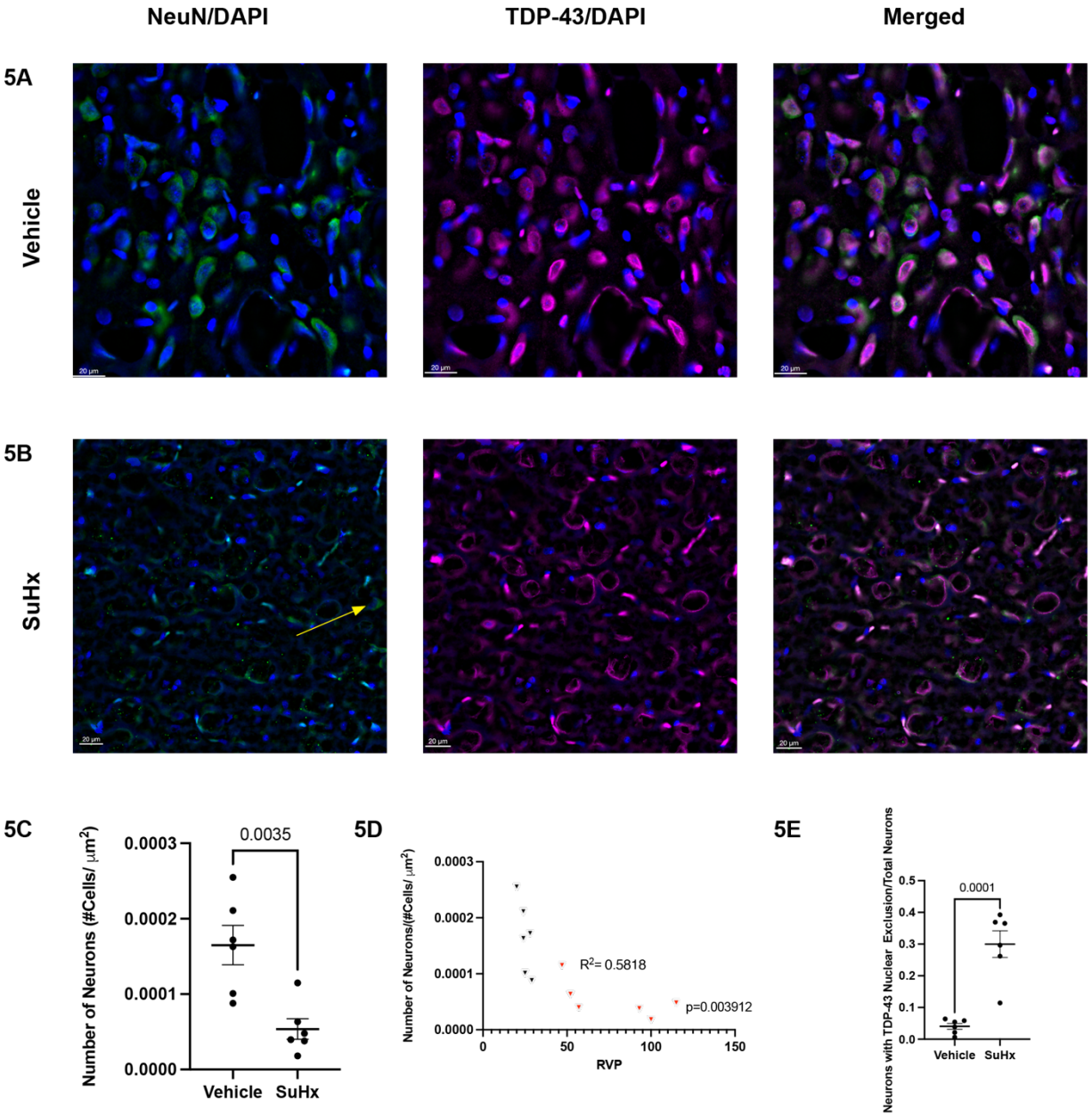

Figure 5. Sugen/hypoxia treatment reduces cortical neuronal density and induces neuronal TDP-43 mislocalization. Representative immunofluorescence images of cortical neurons stained for NeuN (neuronal marker) and DAPI (nuclear marker), TDP-43 and DAPI, and merged channels in rats exposed to vehicle at 40x magnification (**5A**) compared to sugen/hypoxia-treated rats (SuHx). The yellow arrow highlights dysmorphic neurons in SuHx-treated rats (**5B**). Quantification reveals a significant reduction in neuronal density in SuHx-treated rats (n=6) relative to vehicle controls (n=6), with a mean difference of $-0.0001113 \pm 2.937 \times 10^{-5}$ ($p = 0.0035$) (**5C**). Linear regression analysis indicates that right ventricular pressure significantly predicts neuronal density, accounting for 58% of the variance ($R^2 = 0.5825$, $p = 0.0039$). (**5D**). SuHx-treated animals also exhibit significantly increased neuronal TDP-43 nuclear exclusion compared to controls, with a mean difference of 0.2592 ± 0.04323 ($p < 0.0001$) (**5E**). Data are presented as mean ± SEM and analyzed using unpaired two-tailed t-tests unless otherwise specified.

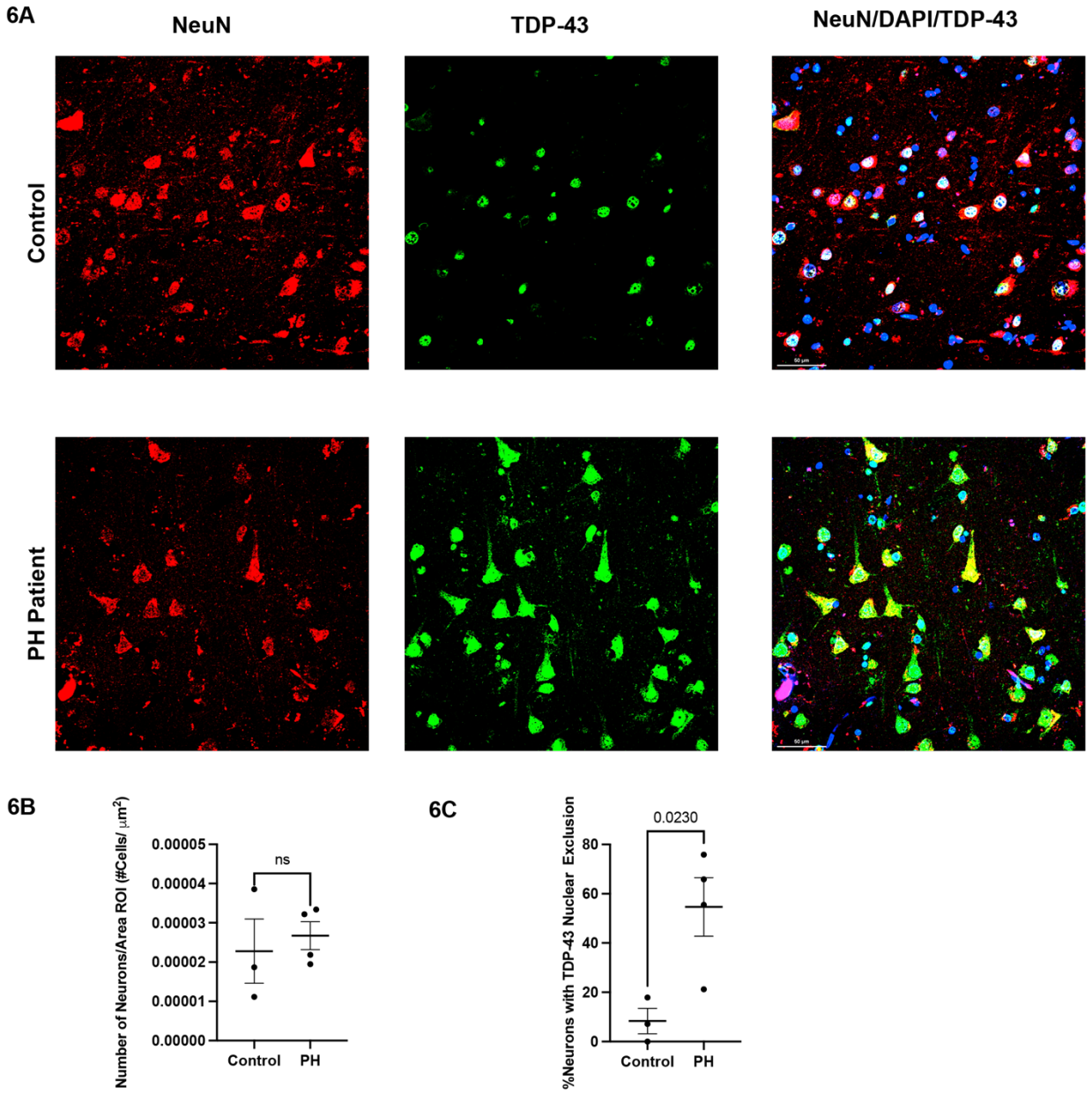

Figure 6. Clinical pulmonary hypertension is associated with increased neuronal TDP-43 mislocalization. Representative immunohistochemistry of frontal cortex tissue from patients with pulmonary hypertension (PH) and age-matched control subjects was used to assess neuronal density and TDP-43 localization (**6A**). Quantitative analysis revealed no significant difference in cortical neuronal density between PH and control groups (**6B**). However, PH subjects (n = 4) demonstrated significantly increased neurons with extranuclear TDP-43compared to controls (n = 3), with a mean difference of 46.27 ± 12.96 (p = 0.0230; **6C**). Scale bar = 50 μm. Data are presented as mean ± SEM and analyzed using a two-tailed unpaired t-test.

499

7A

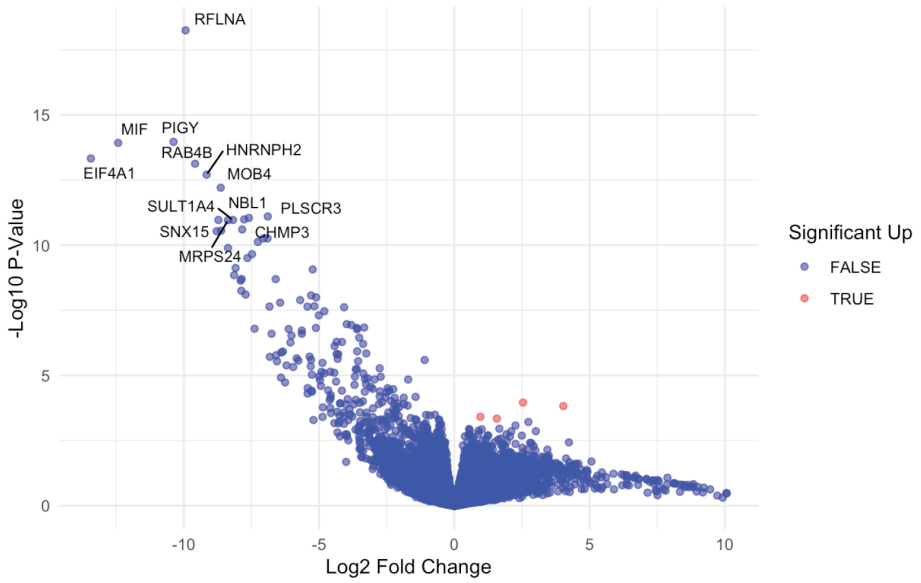

7B

Gene	Name	Function
RFLNA	Refilin A	Actin filament organization
EIF4A1	Eukaryotic Translation Initiation Factor 4A1	RNA polymerase II regulation
MIF	Macrophage Migration Inhibitory Factor	Inflammation
PIGY	Phosphatidylinositol Glycan Anchor Bio-synthesis Class Y	Biosynthesis of glycosylphosphatidylinositol (GPI)
RAB4B	Ras-Related GTP-Binding Protein 4b	Involved in glucose import
HNRNPH2	Heterogeneous Nuclear Ribonucleoprotein H2	Pre-mRNA processing
MOB4	MOB Family Member 4	Oocyte maturation
SULT1A4	Sulfotransferase Family 1A Member 4	Sulfate conjugation
SNX15	Sorting Nexin 15	Intracellular traficking
NBL1	DAN Family BMP Antagonist	BMP antagonist
MRPS24	Mitochondrial Ribosomal Protein S24	Protein synthesis
PLSCR3	Phospholipid Scramblase 3	Apoptosis
CHMP3	Charged Multivesicular Body Protein 3	Sort proteins into multivesicular body pathway

Figure 7. Differential expression of TDP-43 target genes in pulmonary artery endothelial cells from PH dataset. Volcano plot showing differential gene expression from single-cell RNA sequencing of pulmonary artery endothelial cells (PAECs) in PH (n=20) vs control (n=3) (GSE243193). Fisher exact test confirmed that TDP-43–regulated genes were disproportionately downregulated in PH ($p < 2.2 \times 10^{-16}$, OR: 0.193, 95% CI: 0.139-0.269) (**7A**). Manual annotation of top dyresgulated genes provided (**7B**).

Antibody	Dilution	Manufacturer	Product ID
Ionized calcium-binding adaptor molecule 1 (Iba1)	1:500	Synaptic Systems	#234009
Glial Fibrillary Acidic Protein (GFAP)	1:1000	Invitrogen	#13-0300
TDP-43	1:500	Proteintech	#10782-2
Neuron-Specific Nuclear Protein (NeuN)	1:1000	Antibodies.com	#A270544

Supplemental Table 1. Antibodies, dilution, manufacturer, and product ID utilized in immunohistochemistry experiments.

Age	Sex	PH Etiology	PH Severity (RVP)	Comorbidities
69	F	Control	UA	UA
27	F	Control	UA	UA
64	F	Control	UA	UA
83	M	CTEPH	UA	UA
69	M	PoPH	43 mmHg	ESRD, NASH cirrhosis
47	M	PoPH	52 mmHg	AUD, cirrhosis, DM2, hepatic encephalopathy
43	F	SLE-PH	93 mmHg	stroke, ITP, DVT

Supplemental Table 2. Pulmonary hypertension subject demographics. Abbreviations include; unavailable (UA), Chronic Thromboembolic Pulmonary Hypertension (CTEPH), Portal pulmonary hypertension (PoPH), end stage renal disease (ESRD), non-alcoholic steatohepatitis (NASH), alcohol use disorder (AUD), diabetes mellitis 2 (DM2), autoimmune thrombocytopenic purpura (ITP), deep venous thrombosis (DVT).

500

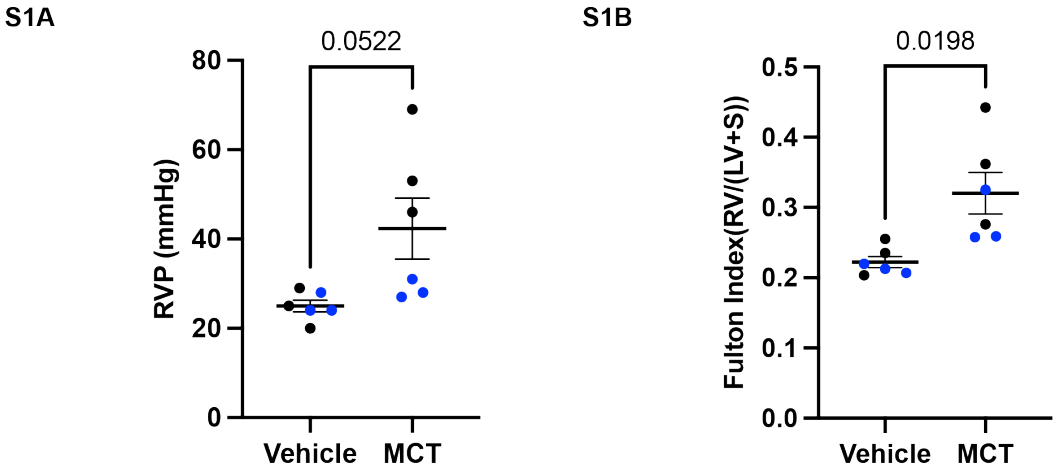

Supplemental Figure 1. Monocrotaline induces vascular remodeling.
Rats treated with monocrotaline (MCT; n = 6) trend to an increased right ventricular pressure (RVP), with a mean difference of 17.33 ± 6.98 mmHg compared to vehicle controls (n = 6; p = 0.0522) (**S1A**). MCT-treated rats demonstrate right ventricular hypertrophy, with a mean Fulton Index difference of 0.09815 ± 0.03066 compared to controls (p = 0.0198) (**S1B**). Data analyzed using a two-tailed unpaired t-test and are presented as mean ± SEM. Female animals depicted in blue.

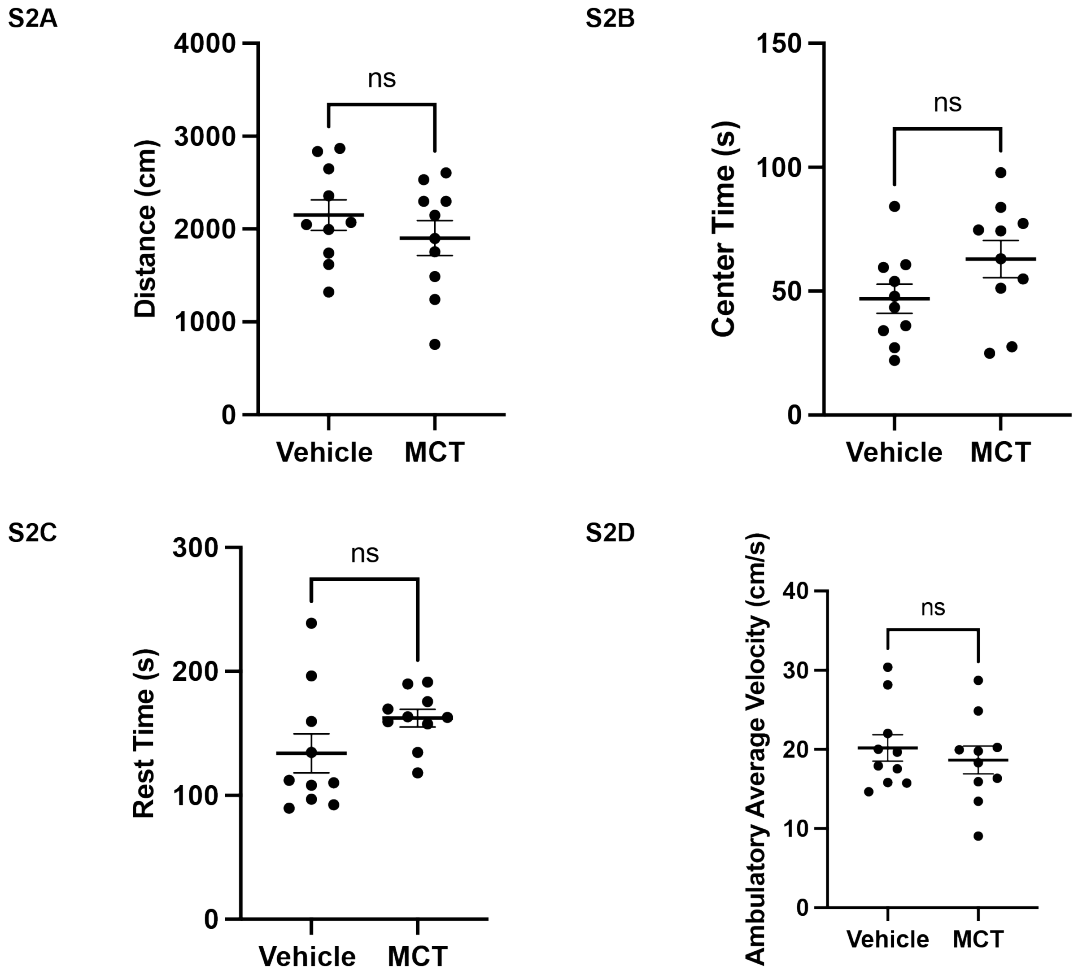

Supplemental Figure 2. Monocrotaline does not induce sickness behavior in rats undergoing open field test. Rats exposed to Monocrotaline (MCT, n = 10) did not exhibit significant differences in behavioral parameters compared to vehicle-treated controls (n = 10). Specifically, there were no significant changes in total distance traveled (**S2A**), time spent in the center of the open field test (**S2B**), time spent at rest (**S2C**), or average ambulatory velocity (**S2D**). Data were analyzed using an unpaired two-tailed t-test and are presented as mean ± SEM.

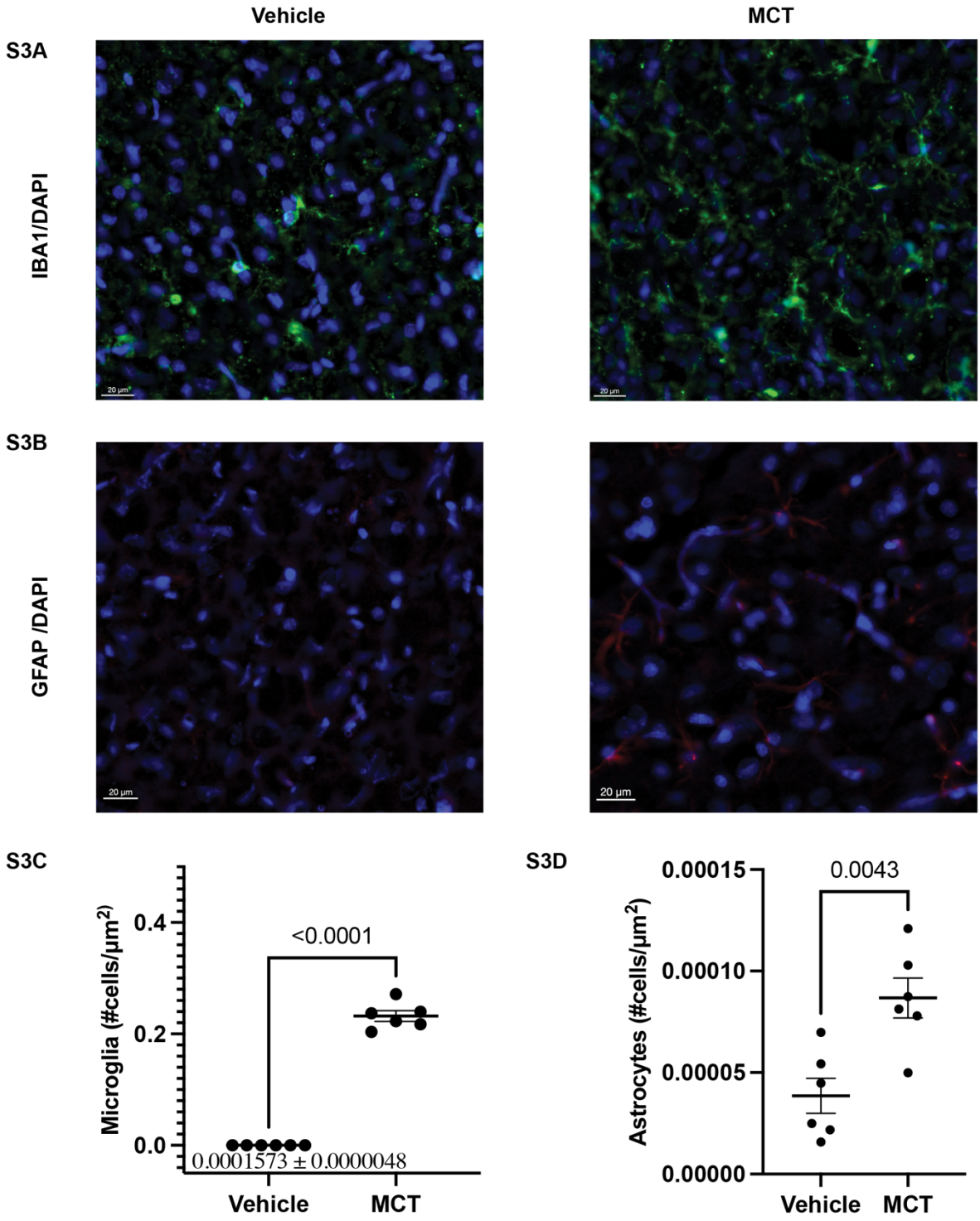

Supplemental Figure 3. Monocrotaline increases cortical gliosis. Representative immunofluorescence images of frontal cortex microglia (IBA1/DAPI) (**S3A**) and astrocytes (GFAP/DAPI) (**S3B**) in rats exposed to monocrotaline (MCT) or vehicle. MCT-treated rats (n = 6) exhibited a significantly increased microglial density (0.2320 ± 0.009541) compared to vehicle-treated controls (n = 6; $p < 0.0001$). (**S3C**). Similarly, astrocyte density was elevated in MCT-treated animals ($4.822 \times 10^{-5} \pm 1.309 \times 10^{-5}$) relative to controls ($p = 0.0043$) (**S3D**). Data are presented as mean ± SEM and were analyzed using a two-tailed unpaired t-test. Error bars are shown for all groups; however, the control group's error bars are not visible at this scale due to extremely low variance (mean = 0.0001573, SEM = 0.0000048) and large difference from the MCT group. A text label is included to indicate the control mean ± SEM.

503

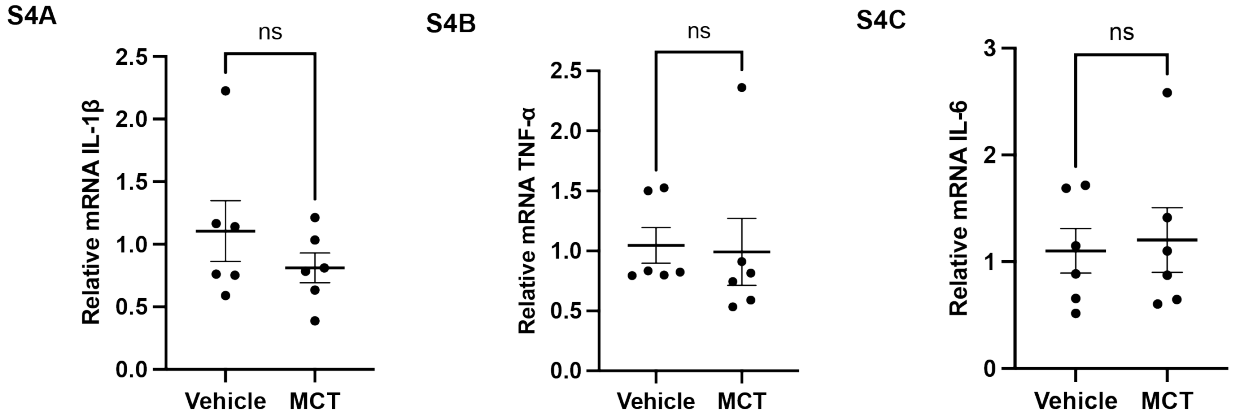

Supplemental Figure 4. Monocrotaline does not increase cortical cytokine expression. Quantitative PCR analysis of cortical cytokine mRNA expression in rats treated with monocrotaline (MCT; n = 6) or vehicle (n = 6) revealed no significant differences in IL-1β (**S4A**), TNF-α (**S4B**), or IL-6 (**S4C**) transcript levels. Data are presented as mean ± SEM and were analyzed using a two-tailed unpaired t-test.

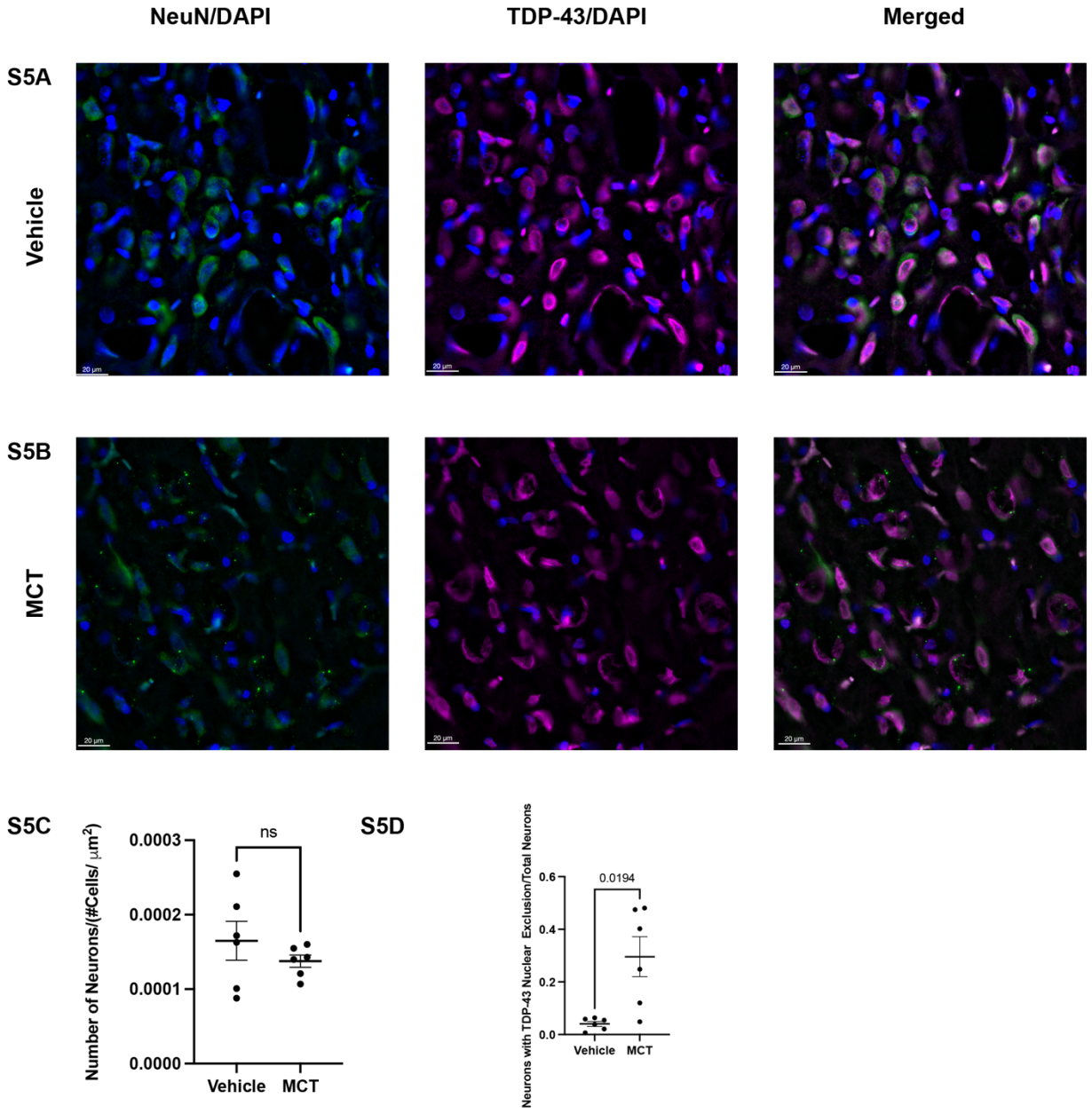

Supplemental Figure 5. Monocrotaline treatment reduces cortical neuronal density and induces neuronal TDP-43 mislocalization. Representative immunofluorescence images of cortical neurons stained for NeuN (neuronal marker) and DAPI (nuclear marker), TDP-43 and DAPI, and merged channels in rats exposed to vehicle at 40x magnification (**S5A**) compared to monocrotaline-treated rats (MCT) (**S5B**). Quantification reveals no change in cortical neuronal density in MCT-treated rats (n=6) compared to vehicle controls (n=6) (**S5C**). MCT-treated animals exhibit significantly increased neuronal nuclear TDP-43 exclusion compared to controls, with a mean difference of 0.2553 ± 0.07623 ($p = 0.0194$) (**S5D**). Data are presented as mean ± SEM and analyzed using unpaired two-tailed t-test.

504